Electronic structure methods for studying surface-enhanced Raman scattering

Lasse Jensen,*[a] Christine M. Aikens[b] and George C. Schatz[c]

Received 16th January 2008
First published as an Advance Article on the web 10th March 2008
DOI: 10.1039/b706023h

This *critical review* highlights recent advances in using electronic structure methods to study surface-enhanced Raman scattering. Examples showing how electronic structure methods, in particular time-dependent density functional theory, can be used to gain microscopic insights into the enhancement mechanism are presented (150 references).

I. Introduction

The interactions between light and metallic nanostructures have long been of great technological and fundamental interest. A key property of metallic nanostructures is the possibility of collective excitation of the conduction electrons by UV-visible light. This excitation, known as *surface plasmon excitation*, is responsible for the remarkable size/shape/environment-dependent optical properties of metallic nanostructures.[1,2] These optical properties were a hindrance to the characterization of colloidal materials in the past as the broad range of shapes and sizes of particles that are typically made resulted in significant heterogeneous broadening in extinction spectra. However advances in colloidal synthesis methods and nanofabrication techniques such as e-beam and nanosphere lithography now allow for the fabrication of well-defined nanoparticles and therefore more homogeneous optical properties.[3–8] In addition, the characterization of the nanoparticles in combination with detailed quantitative electromagnetic simulations has enabled the synthesis of particles with predetermined spectral attributes.[3,4,6,7] This control of the optical properties of nanomaterials has resulted in a wide range of applications in ultra-sensitive chemical and biological sensing.[9–15]

In addition to the intense absorption and scattering of the nanoparticles, plasmon excitation leads to strongly enhanced electromagnetic fields near the nanoparticle surfaces, and this is responsible for the electromagnetic contribution to the Raman signals observed in surface-enhanced Raman scattering (SERS).[9,16–18] Although SERS was discovered several decades ago[19–21] a complete picture of the enhancement mechanism is not available, due to its highly complicated experimental conditions (roughened surfaces, nanoparticle aggregates, molecules that are chemically interacting with the surface, *etc.*). This problem has become even more apparent in the past decade due to the discovery of single molecule SERS which gives rise to the possibility of 10^{10} enhancement factors or more.[22–25] However it is still well accepted that in most cases the strongest enhancement stems from enhanced electromagnetic fields at the surfaces of the partices due to plasmon resonance excitation.[16,17,26,27] Despite this qualitative understanding, developing a theory which describes SERS, including the poorly understood chemical contributions,

[a] *Department of Chemistry, The Pennsylvania State University, 104 Chemistry Building, University Park, PA 16802, USA. E-mail: jensen@chem.psu.edu*
[b] *Department of Chemistry, Kansas State University, 111 Willard Hall, Manhattan, KS 66506-3701, USA*
[c] *Department of Chemistry, Northwestern University, 2145 Sheridan Road, Evanston, IL 60208-3113, USA*

Lasse Jensen received his Cand.Scient. from the University of Copenhagen, Denmark in 2000 and his PhD in 2004 from the University of Groningen, The Netherlands. From 2004–2007 he was a post-doctoral fellow in the group of George C. Schatz and is currently an Assistant Professor of Chemistry at the Pennsylvania State University. His research interest focuses on developing theoretical methods to understand optical spectroscopy of bio- and nano-systems.

Christine M. Aikens received her BS in Chemistry from the University of Oklahoma in 2000. She received a National Science Foundation Predoctoral Fellowship to study at Iowa State University under the direction of Mark Gordon. Upon completion of a PhD in Physical Chemistry in 2005, she moved to Northwestern University to work as a post-doctoral fellow under George C. Schatz. She is currently an Assistant Professor of Chemistry at Kansas State University where her research interests include investigating the self-assembly and optical properties of nanostructured systems.

George C. Schatz is Charles E. and Emma H. Morrison Professor of Chemistry at Northwestern University. He did his BS at Clarkson University and PhD at Caltech, both in chemistry. He was a postdoc at MIT, and has been at Northwestern since 1976. He is a theoretician who studies the optical, structural and energetic properties of nanomaterials and has also contributed to theories of dynamical processes important in chemistry, including gas phase and gas/surface reactions, energy transfer processes, transport phenomena and photochemistry. In the field of nanoscience he has specialized in computational electrodynamics studies of noble metal nanoparticles, nanoholes and other nanostructured materials, he has contributed to theories of DNA melting and nanoparticle aggregates, and he has studied the mechanical properties of nanotubes and thin films. Professor Schatz is a member of the National Academy of Sciences (2005), the American Academy of Arts and Sciences (2002), the International Academy of Quantum Molecular Sciences (2001) and is Editor-in-Chief of the Journal of Physical Chemistry.

remains an important goal, as the combination of a rich vibrational spectrum characteristic of Raman scattering with a strong enhancement makes SERS an attractive method for studying the properties of molecules absorbed on surfaces, and for sensing applications.

A great deal of progress has been made recently in the accurate and efficient calculation of nanostructure optical properties.[28,29] Numerical methods such as the discrete dipole approximation[28] and finite-difference time-domain methods[29] have been used to calculate the plasmonic properties of complex shapes and arrangements. These methods have provided detailed insights into the electromagnetic mechanism in SERS.[27] However, they do not provide any information about the chemical enhancement mechanism since the molecule is either treated as a point dipole or ignored completely. Recent theoretical[30] and experimental[31–33] findings indicate that under certain conditions the chemical enhancement mechanism can be much larger than is usually thought. Electronic structure modeling of the molecule–metal cluster interfacial structure and its optical properties on the atomic scale can provide key insight into the type and strength of the bonds between the molecule and the nanoparticles/nanoclusters, the effects of the surface roughness on the atomic scale, the effects of laser excitation wavelength, and overall, the nature of the observed Raman enhancement itself.

This *critical review* highlights recent advances in using electronic structure methods to study SERS, with emphasis on the different contributions to the overall SERS enhancement (*i.e.*, chemical, charge transfer, electromagnetic). In particular, we will discuss recent developments using time-dependent density functional theory to describe the different SERS enhancement mechanisms using small silver and gold clusters as model systems. We will also discuss briefly the use of similar theories to describe surface-enhanced vibrational Raman optical activity and nonlinear scattering processes which are new areas where electronic structure methods are likely to have an important impact.

II. Enhancement mechanisms

Although the exact nature of the enhancement mechanism involved in SERS is not known, it is well accepted that there are two contributions resulting, respectively, from electromagnetic and chemical interactions between the adsorbate and the metal nanoparticle. Both will contribute to the total SERS enhancement, and it is not possible experimentally to make a clear separation of their individual contributions. However, from a theoretical point of view one can identify at least four different situations where the SERS signal is enhanced due to a different mechanism (see Fig. 1 for a cartoon illustrating the different enhancement mechanisms):

(a) Enhancement due to ground state chemical interactions between molecule and nanoparticle that are not associated with any excitations of the nanoparticle–molecule system.

(b) Resonance Raman enhancement with the excitation wavelength being resonant with a molecular transition.

(c) Charge-transfer (CT) resonance Raman enhancement with the excitation wavelength being resonant with nanoparticle–molecule CT transitions.

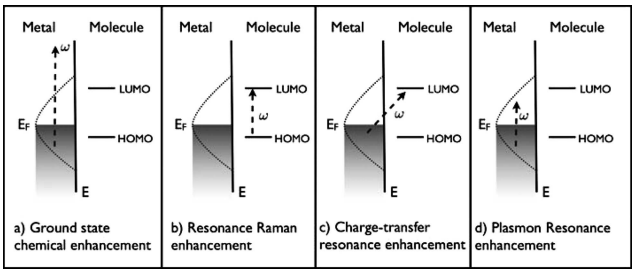

Fig. 1 Illustration of the different types of enhancement mechanism in SERS.

(d) Enhancement due to a very strong local field when the excitation wavelength is resonant with the plasmon excitations in the metal nanoparticle.

We will label these different enhancement mechanisms as CHEM, resonance, CT, and EM, respectively. The first three contributions are often grouped together as the "chemical mechanism" and the last is the "electromagnetic mechanism".[17,26,34] However, we prefer to discuss them separately. It is important to realize that all these enhancement mechanisms are strongly dependent on the Raman excitation wavelength and will therefore only be important for specific wavelengths. The relative importance of these mechanisms is very difficult to establish experimentally since only in certain specific limits can they be separated and studied.

Since the local field enhancement arising from the plasmon excitation can be very large, the electromagnetic mechanism is believed to be the dominant contribution to the observed SERS signal. The strong fields lead to the electrodynamic enhancement mechanism, and it is generally assumed that the SERS signal is enhanced by a factor proportional to the fourth-power of the electric field enhancement, $|E^{\mathrm{loc}}|^4$.[35,36] A straightforward rationale for the field enhancement in SERS can be illustrated by considering the following simple model (here simplified and modified from the original discussion by Gersten and Nitzan).[35]

The Raman scattering of a molecule of interest is affected by the electromagnetic interaction with a polarizable body located close to the molecule. If we consider the molecule and the metal nanoparticle as polarizable objects characterized by polarizabilities α_{M} and α_{NP}, the total polarizability of the system is then given by Silberstein's equations.[37,38]

$$\alpha_{\parallel} = \frac{\alpha_{\mathrm{M}} + \alpha_{\mathrm{NP}} + 4\alpha_{\mathrm{M}}\alpha_{\mathrm{NP}}/R^3}{1 - 4\alpha_{\mathrm{M}}\alpha_{\mathrm{NP}}/R^6}$$

$$\alpha_{\perp} = \frac{\alpha_{\mathrm{M}} + \alpha_{\mathrm{NP}} - 2\alpha_{\mathrm{M}}\alpha_{\mathrm{NP}}/R^3}{1 - \alpha_{\mathrm{M}}\alpha_{\mathrm{NP}}/R^6} \qquad (1)$$

where R is the center-to-center distance between the molecule and the nanoparticle. Note in this equation that we have considered both the case where the field is parallel to the axis between the molecule and particle and where it is perpendicular. The Raman scattering intensity for this system is given by

$$I^{\mathrm{R}} \propto \left|\frac{\partial\alpha}{\partial Q_{\mathrm{M}}}\right|^2 \qquad (2)$$

where Q_M is a normal mode of the molecule. We will assume that the polarizability of the nanoparticle is independent of the normal modes of the molecule, which is reasonable considering that $\alpha_{NP} \gg \alpha_M$. Straightforward differentiation of the polarizability with respect to the normal mode gives

$$\frac{\partial\alpha_{\|}}{\partial Q_M} = \frac{\alpha'_M + 4\alpha_{NP}\alpha'_M/R^3}{1 - 4\alpha_{NP}\alpha_M/R^6} - \frac{\alpha_M + \alpha_{NP} + 4\alpha_{NP}\alpha_M/R^3}{(1 - 4\alpha_{NP}\alpha_M/R^6)^2}(-4\alpha_{NP}\alpha'_M/R^6)$$

$$\frac{\partial\alpha_{\perp}}{\partial Q_M} = \frac{\alpha'_M - 2\alpha_{NP}\alpha'_M/R^3}{1 - \alpha_{NP}\alpha_M/R^6} - \frac{\alpha_M + \alpha_{NP} - 2\alpha_{NP}\alpha_M/R^3}{(1 - \alpha_{NP}\alpha_M/R^6)^2}(-\alpha_{NP}\alpha'_M/R^6) \quad (3)$$

where $\alpha'_M = \frac{\partial\alpha_M}{\partial Q_M}$. After some manipulation the equations can be written as

$$\frac{\partial\alpha_{\|}}{\partial Q_M} = \frac{\alpha'_M(1 + 2\alpha_{NP}/R^3)^2}{(1 - 4\alpha_{NP}\alpha_M/R^6)^2}$$

$$\frac{\partial\alpha_{\perp}}{\partial Q_M} = \frac{\alpha'_M(1 - \alpha_{NP}/R^3)^2}{(1 - \alpha_{NP}\alpha_M/R^6)^2} \quad (4)$$

The Raman intensities are then

$$I^R_{\|} \propto \left|\frac{\partial\alpha_{\|}}{\partial Q_M}\right|^2 = \left(\frac{\partial\alpha_M}{\partial Q_M}\right)^2 \times \frac{(1 + 2\alpha_{NP}/R^3)^4}{(1 - 4\alpha_{NP}\alpha_M/R^6)^4}$$

$$I^R_{\perp} \propto \left|\frac{\partial\alpha_{\perp}}{\partial Q_M}\right|^2 = \left(\frac{\partial\alpha_M}{\partial Q_M}\right)^2 \times \frac{(1 - \alpha_{NP}/R^3)^4}{(1 - \alpha_{NP}\alpha_M/R^6)^4} \quad (5)$$

The denominator in eqn (5) is essentially unity, since the polarizability of the molecule is much less than the polarizability of the nanoparticle and the polarizability of the nanoparticle is proportional to d^3, where d is a measure of the size of the particle (linear dimension). The field enhancement at the molecule due to the metal nanoparticle is $E^{loc}_{\|} = 1 + \frac{2}{r^3}\alpha_{NP}$ and $E^{loc}_{\perp} = 1 - \frac{1}{r^3}\alpha_{NP}$. Using this, the Raman intensity can be expressed as

$$I^R_{\|} = I^{Molecule}_R|E^{loc}_{\|}|^4$$
$$I^R_{\perp} = I^{Molecule}_R|E^{loc}_{\perp}|^4 \quad (6)$$

where $I^{Molecule}_R = \left(\frac{\partial\alpha_M}{\partial Q_M}\right)^2$ is the Raman intensity of the isolated molecule. Thus, the Raman enhancement due to the electromagnetic mechanism depends on the fourth power of the field enhancement factor arising from the polarizable nanoparticle. This applies for both the parallel and perpendicular fields, although the "+2" factor in the parallel case leads to larger field enhancements than the "−1" factor in the perpendicular case (by a factor of 16 in the limit where $\left|\frac{1}{r^3}\alpha_{NP}\right| \gg 1$).

The simple dipole coupling model is useful for qualitative insight, but must be replaced by computational electrodynamics methods such as the DDA and the FDTD methods for a more realistic evaluation of the enhanced local electric field around metal particles. However, even these methods treat the adsorbed molecules as point dipoles or ignore them completely, and thus are incapable of determining the variation in Raman intensity with molecular normal mode. Therefore, we will not discuss these methods in this review. The reader is referred to *e.g.* ref. 27 for a recent overview of these methods.

III. Electronic structure methods for SERS

Despite the success and widespread adoption of the classical electrodynamics models, these models are unable to provide a complete picture of SERS due to the complete neglect of the molecule and the specific interactions between the molecule and the metal surface. To address the chemical interactions between the molecule and the nanoparticle, it is necessary to consider the electronic structure of the molecules. In addition, it is highly desirable to use the same level of electronic structure theory for both the molecule and the metal, and to use an electronic structure model with the capability of determining the optimized geometry of the molecule/metal system in addition to optical properties. Although electronic structure methods are ideal tools for this application, they are restricted by high computational demands and therefore calculations often only consider a few metal atoms, thus limiting their accuracy. In addition, the methods used are often only capable of treating certain aspects of SERS such as their spectra in the static limit, or with frequency dependence included only with two electronic states.

In the following sections, we will discuss various aspects of calculating SERS-relevant information using quantum chemical methods. Our discussion will begin with methods which are limited to the description of a specific enhancement mechanism, but most of our focus will be on newer time-dependent approaches which seek to treat the different enhancement mechanisms in an uniform way, with all the atoms in the molecule and metal described with the same electronic structure model, and including for the full frequency dependence of the electrodynamic response.

A Static Raman calculations

Quantum chemical calculations of static Raman intensities can provide a measure of the CHEM enhancements that arise during analyte adsorption on a metal cluster or surface. Such calculations are particularly useful in describing shifts in the vibrational frequencies of a molecule due to adsorption onto the metal surface. Since this is a property that depends on the local environment rather than the whole metal particle, small cluster models are often sufficient to achieve good agreement with respect to experimental results. The relative Raman intensities depend sensitively on the size, charge, binding site, and orientation of the cluster with respect to the molecule. Therefore, numerous researchers have examined CHEM effects in SERS by employing small metal clusters and semi-empirical, density functional theory, or second order perturbation theory methods. Issues that have been considered include the binding geometry of the adsorbate,[39] the effects of adsorption on various noble and transition metal surfaces,[40] the influence of positively charged atoms at the metal surface,[41,42] the effect of co-adsorbed chloride anions,[43] the consequences of non-zero static electric fields,[44] and the impact of incorporating a continuum solvent in the calculations.[45]

A comprehensive review of these investigations is outside the scope of this review, however we note that static Raman calculations are useful for treating a variety of CHEM enhancement effects, although they are incapable of treating resonant Raman processes and are unable to address the EM enhancement mechanism.

B CT-resonance Raman calculations

The CT mechanism, which arises when incident radiation induces excitation to new metal–adsorbate charge-transfer states, may be considered a chemical effect that is analogous to resonant Raman processes. The theory for this mechanism has been treated in several ways. Adrian used a semi-empirical Wolfsberg–Helmholtz method to investigate metal-to-molecule charge transfer.[46] Lombardi *et al*. included both molecule-to-metal and metal-to-molecule charge transfer in their theory based on a Herzberg–Teller coupling mechanism.[47,48] Using the Peticolas formula,[49] a two-state model connecting the ground state and the CT excited state has been employed to estimate the effect of CT on the relative Raman intensity for pyrazine,[50,51] pyridine,[40,45,52] and pyrimidine.[53] These theories account solely for the CT mechanism and often only consider the relative changes in the Raman intensities, thereby not addressing the magnitude of CT enhancement. An important uncertainty with this type of model is the width of the CT excited state, as this plays a major role in determining the size of the SERS enhancement factor. We will discuss this issue in more detail later as it also arises with the time dependent methods for describing SERS.

C A combined electromagnetic–quantum chemical method

In the hybrid approach of Corni and Tomasi, a system composed of a molecule adsorbed on a cluster of metal particles is divided into three layers that are described at different levels of accuracy.[54] At the first level, the cluster of metal particles is treated as a collection of spherical metal particles described as polarizable dipoles. At the second level, the complex-shaped metal particles in a particular region are treated by applying the theory of integral equations to the Poisson equation using a boundary elements method,[55] which accounts for effects on the electric field due to the complex shape of the particle but neglects the detailed atomic and electronic structure of the metal. At the third level, a time dependent Hartree–Fock (TDHF) approach is used to describe the molecule and the effects of the electric field acting on the molecule due to the electrostatic interaction with the metal particles. This type of approach assumes that the quasistatic approximation is reasonable for investigating the interaction of the incident electric field with the molecule–metal particle system. While the method accounts for the electromagnetic interactions between the metal and the molecule it neglects the specific CHEM interactions. The approach is therefore unable to address the CHEM and CT enhancement mechanism. Although, the model could in principle be extended to a supermolecule (molecule + a small metal cluster) which could account for the specific interactions, thus far it has not been done.

D Resonance Raman calculations

In order to treat both CHEM and EM effects using electronic structure methods, it is crucial to consider derivatives of frequency-dependent polarizabilities near electronic resonances in the system. One of the earliest efforts in this direction involved the investigation of frequency-dependent polarizability derivatives *via* TDHF calculations for an H_2 molecule adsorbed on small Li_n (n = 2, 4, 6) clusters.[56,57] The authors predicted that the Raman intensities of the adsorbate would be enhanced by 10^3–10^4 when the clusters are irradiated at frequencies corresponding to metal cluster excitation energies. More recent work with a similar TDHF approach has extended these calculations to the consideration of more realistic molecule–metal combinations, including CO on Ag_2, Ag_{10}, K_2, Pd_2, and MgO clusters;[58] however the TDHF approach is not capable of describing electronic spectra very accurately (1 eV errors are common) and limitations on system size have generally made it difficult to assess the significance of the results obtained.

In TDDFT, the frequency-dependent polarizability is calculated from the first-order change in the electron density due to a frequency-dependent electric field by solving a set of linear (response) equations.[59,60] While this procedure works well for frequencies well below any electronic excitations, it becomes divergent for frequencies close to a resonance. This can be avoided by including the finite lifetime ($T = 1/\Gamma$) of the electronic states in the normal response formalism.[61–63] The inclusion of the finite lifetime (or damping) allows for the calculation of the real and imaginary polarizabilities over the whole frequency range. In the following section, we will discuss the combination of TDDFT with a short-time approximation to the Kramers, Heisenberg, and Dirac formalism for Raman scattering. Using this method, it is possible to calculate both normal Raman scattering (NRS) and resonance Raman scattering (RRS) intensities from the geometrical derivatives of the frequency-dependent polarizability (real or complex).[64–66]

1 TDDFT short time approximation. In a back scattering or forward scattering geometry, the Raman intensities are given by[67]

$$I(180^\circ) = \frac{\mathrm{d}\sigma}{\mathrm{d}\Omega}(180^\circ) = K_p\left[\frac{90\alpha_p^2 + 14\beta(\alpha)_p^2}{90}\right] \qquad (7)$$

where α_p^2 and $\beta(\alpha)_p^2$ are the isotropic and anisotropic invariants of the dipole–dipole polarizability transition tensor. The parameter K_p, which is independent of the experimental setup but depends on both the incident and scattered frequencies, is given by

$$K_p = \frac{\pi^2}{\varepsilon_0^2}(\tilde{\upsilon}_{\mathrm{in}} - \tilde{\upsilon}_p)^4 \frac{h}{8\pi^2 c\tilde{\upsilon}_p} \frac{1}{1 - \exp[-hc\tilde{\upsilon}_p/k_{\mathrm{B}}T]} \qquad (8)$$

where $\tilde{\upsilon}_{\mathrm{in}}$ and $\tilde{\upsilon}_p$ are the frequencies of the incident light and of the p'th vibrational mode, respectively.

The different invariants contributing to the Raman intensities consist of tensor contractions of the dipole–dipole

polarizability transition tensor, $\alpha^p_{\alpha\alpha}$, and are given by

$$\alpha_p^2 = \frac{1}{9}\alpha^p_{\alpha\alpha}\alpha^{p*}_{\beta\beta} \tag{9}$$

$$\beta(\alpha)_p^2 = \frac{1}{2}(3\alpha^p_{\alpha\beta}\alpha^{p*}_{\alpha\beta} - \alpha^p_{\alpha\alpha}\alpha^{p*}_{\beta\beta}) \tag{10}$$

The Einstein summation convention is adopted for repeated Greek subscripts, *i.e.*, a Greek subscript denotes x, y or z in a Cartesian coordinate system.

In order to calculate the polarizability transition tensors, one typically adopts the Placzek approximation which is in general valid in the off-resonance case. However, by adopting a short-time approximation one can formulate a Placzek-like polarizability theory which is valid both on- and off-resonance.[64–66,68–70] Within the Born–Oppenheimer approximation the polarizability transition tensor from an initial vibrational state $|I,\ 0\rangle$ to a final state $|F,\ 0\rangle$ of the electronic ground state is given using atomic units by[71,72]

$$\alpha^p_{\alpha\beta} = \sum_{k\neq 0}\sum_J \frac{\langle F,0|\langle 0|\mu_\alpha|k\rangle|J,k\rangle\langle J,k|\langle k|\mu_\beta|0\rangle|I,0\rangle}{E_k^J - E_0^I - \omega - i\Gamma} + \frac{\langle 0|\mu_\alpha|k\rangle|J,k\rangle\langle J,k|\langle k|\mu_\beta|0\rangle}{E_k^J - E_0^I + \omega_S + i\Gamma} \tag{11}$$

where E_k^J is the energy for the $|J,k\rangle$ state, ω is the energy of the incident light and ω_S of the scattered light. The sum over k and J is over all the Born–Oppenheimer electronic surfaces $|k\rangle$ and all the vibrational levels within each surface $|J,\ k\rangle$. In the short-time approximation, it can then be shown that the vibrational energy contribution in the denominator can be ignored[64–66,68–70]

$$\alpha^p_{\alpha\beta} = \langle F,0|\alpha_{\alpha\beta}|I,0\rangle = \left\langle F,0\left|\left(\sum_{k\neq 0}\frac{\langle 0|\mu_\alpha|k\rangle\langle k|\mu_\beta|0\rangle}{E_k - E_0 - \omega - i\Gamma} + \frac{\langle 0|\mu_\alpha|k\rangle\langle k|\mu_\beta|0\rangle}{E_k - E_0 + \omega + i\Gamma}\right)\right|I,0\right\rangle \tag{12}$$

where we have removed the sum over vibrational states for each electronic state since $\sum_J |J,k\rangle\langle J,k| = 1$. Lastly, we have replaced ω_S with ω in the second term since at resonance the first term is dominant. In order for the short-time approximation to be valid, Γ should be large, *i.e.* excited state dephasing that is rapid compared to the vibrational time scale. Therefore, molecules which show significant vibrational structure in their absorption spectrum will also exhibit vibrational structure in their Raman spectrum which cannot be described within the short-time approximation.

The transition tensors are then expanded in a Taylor series around the equilibrium geometry. In the harmonic approximation, the first term in the expansion accounts for Rayleigh scattering and the second term for the fundamental Raman scattering. The transition tensors can then be expressed as geometric derivatives of molecule properties as

$$\alpha^p_{\alpha\beta}\alpha^p_{\alpha\beta} = \langle 1_p|\alpha_{\alpha\beta}|0\rangle\langle 0|\alpha_{\alpha\beta}|1_p\rangle = \left(\frac{\partial\alpha_{\alpha\beta}}{\partial Q_p}\right)_0\left(\frac{\partial\alpha_{\alpha\beta}}{\partial Q_p}\right)_0|\langle 1_p|Q|0\rangle|^2 \tag{13}$$

where Q_p is the normal mode of the p'th vibration. If we assume a two-state model, *i.e.* one electronic excited state, the electric dipole–dipole polarizability is given by[66]

$$\frac{\partial\alpha^{TS}_{zz}}{\partial Q_p} = -\frac{F_{zz}}{(\omega_{eg} - \omega - i\Gamma)^2}\left(\frac{\partial\omega_{eg}}{\partial Q_p}\right) \tag{14}$$

where F_{zz} is the dipole oscillator strength and ω_{eg} is the excitation energy. At resonance, the Raman intensities in the two-state approximation are then simply given by

$$I(180^\circ) = K_p\frac{24}{90}\mathrm{Re}(\alpha^p_{zz}\alpha^{p*}_{zz}) \propto \frac{F_{zz}F_{zz}}{\Gamma^4}\left(\frac{\partial\omega_{eg}}{\partial Q_p}\right)^2 \tag{15}$$

which is identical to the excited-state gradients approximation for calculating RRS.[73] However, in general the method is used without assuming a two-state approximation. The two-state approximation shows that the resonance Raman intensities depend on the damping parameter as $1/\Gamma^4$, so it should be clear that the excited state width plays a crucial role in determining SERS intensities. It is also important to realize that this expression also holds for the CT enhancement mechanism, so the choice of the width for this mechanism, and whether it should be the same or different than for the resonance Raman mechanism is important.[48] Values of Γ are related to the absorption line shape and the resonance Raman excitation profile, and can be estimated from experimental absorption spectra (if available). However, one should realize that there is also a contribution arising from solvent dephasing if the data correspond to a molecule in the condensed phase.[74,75] However, if the excitation is weak or overlapping with other transitions, it is difficult to accurately extract information about Γ from the absorption spectrum.

IV. Enhanced Raman properties of small metal clusters

Although metallic nanoparticles are well described using classical electrodynamics, deviations occur when the particle sizes become smaller than $\sim$10 nm.[18,76–79] For these small particles, quantum size effects become important and an increase in surface scattering of the conduction electrons causes the plasmon band to be strongly damped and broadened. As the particle size decreases further ($<$2 nm), the classical description is no longer valid since the particle shows molecular-like electronic structure due to its low density of states. In this regime the plasmon band is replaced with discrete electronic transitions.[80–82] Therefore, first-principles modeling combined with available experimental spectroscopic data is necessary to understand the electronic structure and optical properties of small clusters of different sizes.[18,78,79,83,84]

While it is mainly the absorption and emission properties that have been studied, the Raman scattering properties of small clusters have been studied using a combination of resonance Raman spectroscopy and first-principles calculations.[85–87] This has been shown to provide more detailed information about cluster structure than what is available from absorption spectra. Recently Dickson *et al.*[88] have performed measurements which suggest that small (2–8 atom) silver clusters encapsulated in a dendrimer or peptide scaffold

can produce single-molecule Raman scattering characteristic of the scaffold. This result is quite surprising since single molecule Raman has only been observed for molecules adsorbed onto large nanoparticles (>30 nm) in past work, where the strongly enhanced local field near the nanoparticle surface due to plasmon excitation is expected to be operative.[22–25] Using near-infrared light, Price and Whetten[89] obtained Raman spectra of benzenethiole monolayer protected gold nanoclusters with core diameters of ~1.7 and ~1.5 nm. They found selective enhancement of several vibrational modes although the enhancement factors were not quantified.

In the following sections, we will highlight recent studies using TDDFT to calculate the Raman properties of molecules interacting with sub-nm silver and gold clusters. Studying these small metal clusters as model systems for larger particles can provide detailed insights into the nature of molecule-cluster binding and their optical properties. In addition, the small size of these clusters allows for first-principles methods to be used, thereby enabling a consistent treatment of the different enhancement mechanisms which can provide microscopic insights into SERS.

A Silver clusters

Many experimental and theoretical studies have been performed to address the structural, electronic, and optical properties of small silver clusters.[18,78,79,83,84,90–94] Theoretical studies of the structure and absorption spectra of small Ag_n clusters ($n \leq 9$) show that the most stable structures have topologies which are similar to the corresponding sodium clusters, and that the structures of Ag_n are planar up to $n = 6$.[90,91,93] For larger clusters, this direct comparison becomes cumbersome since there exist many local minima close in energy and the global minimum might not be the spectroscopically relevant configuration due to matrix or temperature effects.

1 Absorption properties. Photoabsorption studies[95] of small silver clusters (2–21 atoms) embedded in rare-gas matrices have shown that the spectra of the smaller clusters have several discrete peaks whereas the larger clusters are dominated by a single broad peak. As an example of the latter, the Ag_{20} cluster in an argon matrix is dominated by a broad peak with a maximum at 3.70 eV.[95] Although this broad absorption feature cannot be considered as a true collective excitation due to the small size of the cluster, it can be considered as a microscopic analog to the plasmon excitation observed in nanoparticles, with strong dipolar excitation that will produce a field close to the nanoparticle which is capable of enhancing Raman scattering.

Recently, TDDFT has been used to calculate the absorption and Raman scattering of the Ag_n–pyridine ($n = 2, 4, 6, 8, 20$)[96,97] and Ag_{20}–pyridazine–Ag_{20} model systems.[30] The calculations were done using the BP86 xc-potential and a TZP basis set. In Fig. 2 we show the orbital interaction diagram and the simulated absorption spectrum of the Ag_{20}–pyridine complex. The absorption spectrum is dominated by very strong silver–silver transitions centered around 3.3 eV. This is similar to the 3.7 eV maximum noted above in the experimental spectrum, with the difference likely a reflection of errors in

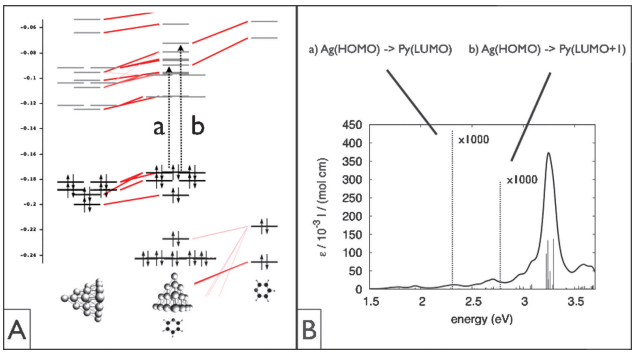

Fig. 2 (A) Orbital interaction diagram for the interaction between the pyridine molecule and the Ag_{20} cluster. (B) The simulated absorption spectrum of the pyridine–Ag_{20} complex. The two transitions labeled a and b correspond to the CT transition from the HOMO of the silver to the LUMO and LUMO + 1 of pyridine, respectively.

TDDFT. The interactions between pyridine and the Ag_{20} cluster also lead to new states which correspond to excitations from the HOMO of the Ag_{20} cluster to the LUMO/LUMO + 1 of the pyridine molecule. These new CT states lie rather low in energy and have very small oscillator strengths. However, it is well known that standard TDDFT calculations underestimate CT excitations in weakly interacting systems and predict the wrong distance dependence.[98] This is related to a deficiency in the adopted exchange–correlation kernel (usually the adiabatic LDA or GGA). Experimentally, the CT excitations of pyridine absorbed on a Ag(111) surface have been observed to be ~1.4–2.4 eV using electron energy loss (EELS),[99] whereas inverse photoemission (IPE) indicates the LUMO and LUMO + 1 to be ~2.9 eV above the Fermi level.[100] On a Cu(111) surface, two photon photoemission (2PPE) finds the unoccupied states of pyridine to be at 3.15 and 3.75 eV above the Fermi level.[101]

2 CHEM enhancement. The use of the short-time approximation in combination with TDDFT enables the calculation of the Raman spectra at wavelengths resonant with the CT transition and the strong silver–silver transitions since the method is not restricted to a two-state approximation. The Raman spectra calculated at different wavelengths allow for a separation of the different contribution to the total SERS enhancement factors. This is illustrated in Fig. 3 where we display the simulated normal Raman spectrum of pyridine, the simulated Raman spectra of the Ag_{20}–pyridine complex at three different wavelengths and the experimental SERS spectrum of pyridine on roughened silver electrodes. The simulated Raman spectra were obtained using the BP86 xc-potential and a TZP basis set. The simulated normal Raman spectrum of pyridine was found to be in good agreement with the experimental spectrum (not shown here) although the two dominant ring breathing modes at 1022 and 979 cm^{-1} were found to be sensitive to both the xc-potential and solvent effects.[96,97] As can be seen from Fig. 3, both the absolute and the relative intensities depend strongly on excitation wavelength. We will discuss the different spectra below in terms of the different enhancements described in section II. The comparison between the off-resonant Raman spectrum of pyridine (Fig. 3A)

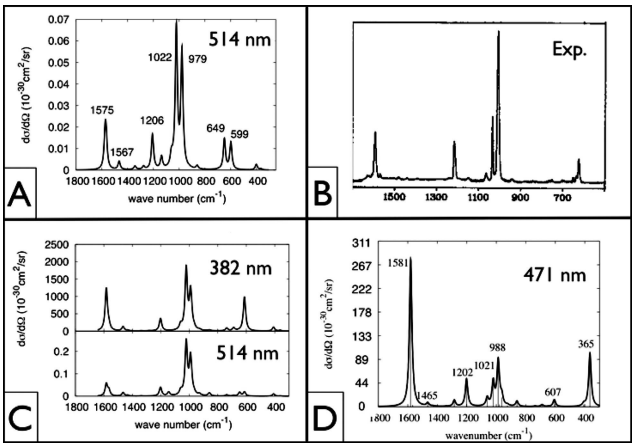

Fig. 3 (A) Simulated normal Raman spectrum of pyridine at 514 nm. Reproduced with permission from ref. 97. Copyright 2007 American Chemical Society. (B) Experimental SERS spectrum of pyridine on roughened silver electrodes. Reused with permission from ref. 102. Copyright 1988, American Institute of Physics. (C) Top: simulated Raman spectrum of the pyridine–Ag_{20} complex at 382 nm; bottom: simulated Raman spectrum of the Ag_{20}–pyridine complex at 514 nm. Reproduced with permission from ref. 97. Copyright 2007 American Chemical Society. (D) Simulated Raman spectrum of the Ag_{20}–pyridine complex at 471 nm. Reproduced with permission from ref. 96. Copyright 2006 American Chemical Society.

with the corresponding spectrum of pyridine–silver complexes (Fig. 3C, bottom spectrum) provides a direct measure of the CHEM enhancements. Moreover, the spectra of the different Ag_n–pyridine complexes appear quite similar to the spectrum of pyridine, with average enhancements that increase slowly with cluster size but are always below a factor of 12. The enhancement was found to correlate with the induced polarizability (*i.e.* the difference in the polarizability of the complex and the sum of the isolated silver cluster and the molecule).[97] This result is not surprising since the polarizability is very sensitive to the electronic structure of the system, and therefore, the induced polarizability reflects to what degree the electronic states of the two systems interact.

3 CT enhancement. The CT enhancement mechanism was probed by calculating the Raman spectrum of the Ag_{20}–pyridine complex using a wavelength resonant with the HOMO to LUMO + 1 CT transition at 471 nm (Fig. 3D).[96] A TZP basis set and the BP86 xc-potential was used in the TDDFT calculations. As expected from the resonance Raman mechanism, significant enhancement of 10^3 on top of the chemical enhancement was found. However, as seen from Fig. 3D the CT enhanced spectra are dominated by the ring stretch mode at 1581 cm^{-1} and the ring twist mode at 365 cm^{-1}, in contrast to the experimental SERS spectrum which is dominated by the two ring breathing modes around 1000 cm^{-1}. Arenas *et al.*[52] analyzed theoretically the CT mechanism for pyridine by considering the displacements between the ground state of pyridine and its anion. Their relative intensities are in good agreement with the findings here, particularly the very strong enhancement of the mode at 1573 cm^{-1}. Although significant CT enhancement is possible, the result in Fig. 3D is most likely an upper-bound since it was obtained with a damping factor taken from the width of the absorption spectra. The real width of the CT excitation could be significantly larger due to the ultra-fast nature of relaxation from the excited state, thereby reducing the enhancement by orders of magnitude.

4 EM enhancement. The electromagnetic enhancement mechanism was probed by calculating the Raman spectrum of the Ag_n–pyridine complex using a wavelength resonant with the strong silver–silver transition (Fig. 3C, top spectra).[96,97] TDDFT calculations were done using a TZP basis set and the BP86 xc-potential. The enhancement and the appearance of the Raman spectrum were shown to have a very strong dependence on cluster size. The total enhancements for the complexes are between 10^3–10^4. The best overall agreement with the experimental SERS spectrum was found for pyridine adsorbed on the faces of the tetrahedral Ag_{20} cluster (see Fig. 3 for the comparison). Assuming a point dipole model similar to that described earlier in section II to calculate the local field at the molecule, it was shown that the enhancement roughly scales as $|E^{loc}|^4 \sim \frac{\alpha_{reso}^4}{R^9}$, where α_{reso} is the polarizability at resonance and R is the distance from the center of the cluster to the nitrogen atom in pyridine. The fact the electric field falls off less rapidly than R^{-3} is expected due to deviation from the point dipole model for geometries corresponding to molecular adsorption directly on the particle surface. Fig. 4 illustrates the off- and on-resonant electric field distributions, $|E|^2$, around a Ag_{20} cluster calculated from the induced density due to an incident electric field using TDDFT. It is clear that there is a significant field enhancement for wavelengths resonant with the strong silver–silver transitions, which is similar to results obtained for larger nanoparticles.[32] Field enhancement on the order of 100 is found in the region where pyridine binds to the surface in good agreement with the 10^3–10^4 enhancement of the Raman cross section.

These results indicate that the absorption properties of a 20 atom silver tetrahedral cluster behave quite similarly to plasmon excitation observed in nanoparticles, and the Raman enhancement due to this cluster is comparable to findings on larger isolated nanoparticles (> 10 nm), at least as far as the traditional SERS enhancement is concerned. Although we find significant "surface" enhanced Raman scattering for pyridine interacting with the small silver clusters, the enhancements are far from what is needed for single molecule SERS measurements. In contrast to the work by Dickson *et al.*[88] which suggested single-molecule Raman scattering for nm size or smaller silver particles, we find enhancements that are similar

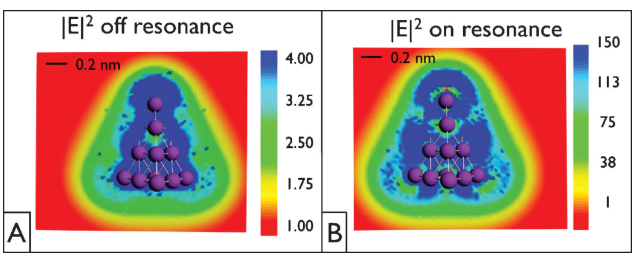

Fig. 4 (A) Off-resonant electric field distribution around an Ag_{20} cluster. (B) Resonant electric field distribution about an Ag_{20} cluster. The electric field distributions are calculating using TDDFT, BP86 and a TZP basis set.

to those for non-single molecule measurements or for molecular resonance Raman scattering. The detailed decomposition in enhancement mechanisms that was used would be further complicated if the molecule had electronic transitions which overlap the metal excitations, but this does not happen in the present case. A good example where such overlap occurs is rhodamine 6G (R6G), which is a typical chromophore used in single-molecule SERS. A recent study shows a strong molecular resonance enhancement of 10^5 for R6G.[103]

5 Molecular junction. Recent theoretical results have indicated the possibility of a large chemical enhancement factor for a molecule at the junction between two nanoparticles.[30] This is particularly interesting since single-molecule SERS is often associated with molecules in junctions. It is generally thought that the very strong enhanced field in junctions between nanoparticles, the so-called hot spots, are the reason for the extraordinary enhancements in single-molecule SERS. Using TDDFT, the absorption and Raman spectra for a pyrazine molecule located at the junction between two tetrahedral Ag_{20} clusters was calculated. The calculations were done using the BP86 xc-potential and a TZP basis set. Pyrazine differs from pyridine by having a second N atom in the *para* position instead of a C–H group. However, the perturbations to the aromatic ring causes pyrazine to bind differently to the silver clusters than pyridine. This directly affects the overall appearance of the Raman spectra making a direct comparison difficult.[30] Fig. 5 shows the absorption and Raman spectra at three different wavelengths. The simulations indicate that the total enhancement factor is of the order of 10^6 with the ground state chemical enhancement factor accounting for as much as 10^5. Tuning of the laser wavelength from off-resonance (514.5 nm, Fig. 5B) to resonance (378 nm, Fig. 5C) changes the Raman intensity by a factor of 5, an enhancement attributed to the EM enhancement mechanism. An incident wavelength of 378 nm leads to excitation parallel to the intercluster axis, while an incident wavelength of 361 nm (Fig. 5D) induces excitation perpendicular to the intercluster axis. According to EM theory, parallel excitation usually experiences constructive interference and the EM enhancement is significant. Perpendicular excitation usually experiences destructive interference and thus little EM enhancement (see eqn (6) in section II). The EM enhancement is only a factor of 5 for this choice of nanoparticle, suggesting that, unlike larger nanoparticles, the junction between these small Ag_{20} tetrahedral clusters does not provide an electromagnetic "hot spot". The reason for this result is apparent from Fig. 4, as this shows that the field around the silver tetrahedron decays to a small value just a few tenths of a nm away from the particle surface. In the case of the junction structure, the two silver particles are separated by a distance that is comparable to the particle size, which means that the field around one particle will have decayed to a small value at the location of the second particle. For larger particles and gaps that are comparable to the one being considered here, decay of the field will be smaller, so much stronger interactions between the particles can occur. Therefore, the enhancements needed for single-molecule SERS can only be obtained for junctions between larger particles and the particle sizes considered here are not large enough to achieve such large enhancements.

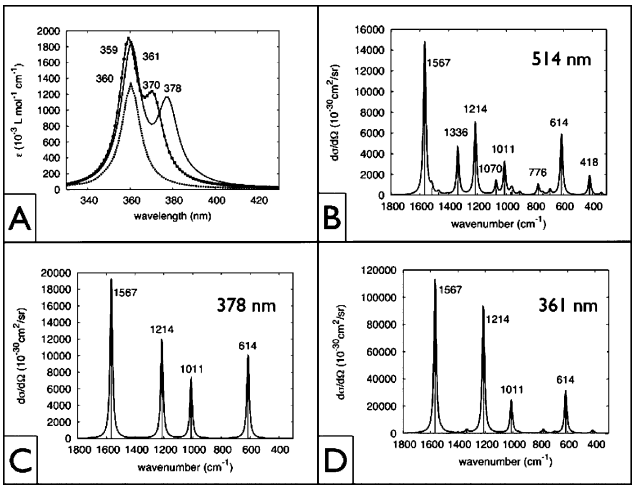

Fig. 5 (A) Simulated absorption spectrum (solid line) of the Ag_{20}–pyrazine–Ag_{20} junction. Reproduced with permission from ref. 30. Copyright 2006 American Chemical Society. For comparison, simulated absorption spectra for the isolated Ag_{20} tetrahedron (dashed line) and junction without molecule (solid line with squares) are also plotted. (B) Simulated normal Raman spectrum of the Ag_{20}–pyrazine–Ag_{20} junction at 514 nm. Reproduced with permission from ref. 30. Copyright 2006 American Chemical Society. (C) Simulated resonance Raman spectrum of the Ag_{20}–pyrazine–Ag_{20} junction at 378 nm. Reproduced with permission from ref. 30. Copyright 2006 American Chemical Society. (D) Simulated resonance Raman spectrum of the Ag_{20}–pyrazine–Ag_{20} junction at 361 nm. Reproduced with permission from ref. 30. Copyright 2006 American Chemical Society.

B Gold clusters

Both silver and gold provide useful SERS substrates, so the differences between these two metals are of interest. The structural, electronic, and optical properties of small gold clusters vary substantially from the properties of small silver clusters. Many of the differences are due to the strong relativistic effects that gold exhibits, which lowers the energy difference between the filled d and partially filled sp orbitals and increases the mixing of these orbitals.[104]

The global minimum energy structures for small Au_n clusters are planar for larger n values than for silver clusters, although the exact planar–nonplanar crossover point for gold is still a subject of debate. [See ref. 105 for a recent discussion of this issue.] The topologies of gold clusters up to $n = 80$ have been studied theoretically using a variety of methods including empirical potentials and density functional theory methods. [See ref. 106 for a recent set of structural references.] The photoelectron spectra (PES) of Au_n ($n = 1$–70 and some selected larger n values) have been measured,[107] and comparison between the experimentally measured and theoretically predicted PES has enabled the determination of structures for some of these clusters,[106,108–111] including the assignment of a tetrahedral structure for Au_{20}.[112]

1 Absorption and PES properties. In addition to structural properties, the optical properties of gold also differ from the optical properties of silver. Thus the measured absorption

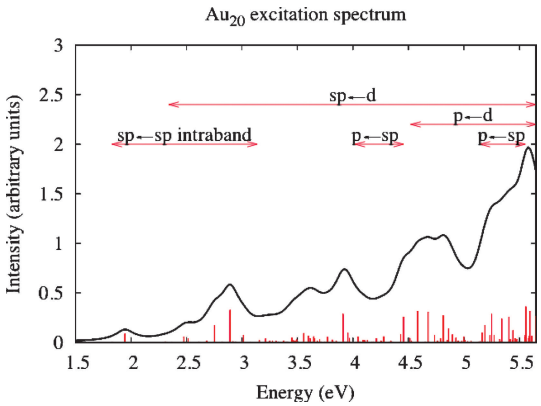

Fig. 6 Optical absorption spectrum of the tetrahedral Au_{20} cluster. Reproduced with permission from ref. 113. Copyright 2006 American Chemical Society. Calculated using TDDFT, BP86 and TZP basis set.

spectra for Au_nXe_m and $Au_nXe_m^+$ (n = 7, 9, 11, 13, and m = 1, 2) consist of a series of small peaks in the 2–6 eV range of excitation energies,[114] and so does the PES spectrum of Au_{20}.[107] The calculated spectrum for Au_{20} (Fig. 6) displays peaks which reasonably match the PES results[113] with intensities that are reduced by over a factor of 10 from the single strong peak that is seen for Ag_{20}. This behavior can be understood as arising from relativistic effects, which cause the intraband (sp ← sp) and interband (sp ← d) transitions to overlap for Au. Thus the single strong intraband absorption feature that we described earlier for Ag is mixed with many interband states in Au clusters, resulting in multiple absorption features that are spread out over a wide range of the vis/UV spectrum, and with a reduction in oscillator strength.

2 CHEM enhancement. Because the optical properties of gold and silver differ, SERS of adsorbates on these metals also differ. One recent TDDFT study[113] compared the SERS mechanisms and enhancement factors for pyridine on the tetrahedral Au_{20} cluster to the previously studied[96,97] pyridine–Ag_{20} system. Pyridine, like many other molecules, binds more strongly to gold than to silver. Binding to low-coordinated sites such as a vertex site tends to increase the binding energy for both gold and silver relative to higher-coordinated sites such as a surface (face) site. These binding properties are important to the usefulness of the SERS technique, as the adsorbate must be located close (generally $<$1 nm) to the metal cluster in order to experience enhancement.

For gold, the optical absorption spectrum (Fig. 6) consists of many peaks that are weak relative to silver. The first significant peak is red-shifted relative to the silver peak (appearing at 2.9 eV in Au_{20} compared to 3.6 eV for Ag_{20}), which is known experimentally for larger particles as well. Because of the broad absorption spectrum, the imaginary polarizability curve for gold is also broader than that for silver. For the tetrahedral Au_{20} structure, CHEM effects lead to a factor of 20 enhancement for adsorption on the vertex site and a factor of 3 enhancement for adsorption on the surface site, which are to be compared with CHEM enhancement factors of 8 and 4 for the respective sites on silver. The increased CHEM enhancement for the vertex site in gold can be correlated with stronger binding interactions.

3 EM enhancement. Experimentally, SERS on silver substrates tends to have an overall enhancement factor that is one or more orders of magnitude larger than SERS on gold substrates (except at wavelengths longer than 750 nm). Similar results have been observed for the Ag_{20} and Au_{20} clusters using TDDFT to examine RRS for the metal–pyridine complex. For pyridine on Ag_{20}, the enhancement factor at the vertex site is 10^3–10^4, while the enhancement factor at the surface site is 10^4.[97] For pyridine on Au_{20}, the enhancement factor at the vertex site is also 10^3–10^4, but the enhancement factor at the surface site is only 10^2–10^3.[113] The vertex site comparison is somewhat anomalous due to the larger CHEM contribution for Au, but the surface site comparison (likely the more significant comparison as surface sites will dominate over vertex sites for larger particles) clearly shows that electromagnetic enhancement effects are larger for silver particles.

4 Field-gradient contributions. As mentioned earlier the EM mechanism of SERS arises because the local electric field in the vicinity of metal nanoparticles and roughened surfaces is greatly enhanced relative to the incident electric field. Near a metal surface, the effects of the local electric field gradient may also be substantial because the normal component of the electric field varies rapidly. However the role of the field gradient on SERS is not completely understood. In the early 1980s, Moskovits and DiLella observed that benzene-d_6 adsorbed on a silver film exhibits seven vibrational modes that are normally inactive in the spectrum of the free molecule.[115] Symmetry-lowering to C_{3v} due to a molecule–surface interaction in which each of the three double bonds in benzene binds to a metal atom could explain the observed modes; however, this usually implies a strong interaction with the surface. Since the frequency shifts in the Raman spectrum are very small, Moskovits *et al.* proposed that the transformation properties of the dipole–quadrupole term could be responsible for the observed modes due to large field gradients at the surface of the metal.[116,117] Polubotko also interpreted the phenomenon in terms of the dipole–quadrupole SERS mechanism.[118] However, Perry, Hatch, and Campion showed that the ratio of the forbidden and allowed modes is independent of excitation wavelength, which suggests that the field gradient mechanism is not important, at least for large molecules physisorbed on a flat surface.[119]

In the multipole polarizability expansion of the dipole moment, the k'th component may be written as

$$\mu_k = \alpha_{km}E_k + \frac{1}{3}A_{k,mn}\frac{\partial E_n}{\partial m} + \cdots \qquad (16)$$

where k, m, and n may be x, y, and z, E_k is a component of the incident electric field, $\partial E_n/\partial m$ is the derivative of the electric field with respect to m, α_{km} is the molecular dipole–dipole polarizability, $A_{k,mn}$ is the dipole–quadrupole polarizability, and Einstein summation is employed. The ratio $A_{k,mn}/\alpha_{km}$ has the units of length, and its magnitude is approximately a molecular dimension.[120] The field gradient mechanism, also called the dipole–quadrupole SERS mechanism, would play a role if the second term in eqn (16) is similar in magnitude to the first.

In a recent study, TDDFT calculations were employed to evaluate the dipole–dipole and dipole–quadrupole polarizabilities of carbon monoxide and pyridine interacting with a Au_{20} cluster.[121] The calculations were done using the BP86 xc-potential and a TZP basis set. Calculations of the dipole–dipole polarizability derivatives described in the previous sections include all possible interactions between the molecule and metal cluster, and thus they include dipole–quadrupole interaction effects between the molecule and metal cluster. The dipole–quadrupole effects over the length scale of the supermolecular (molecule + metal) system are less than 0.005% of the total for systems consisting of a small, chemisorbed molecule interacting with the tetrahedral Au_{20} cluster under both resonant and non-resonant conditions.[121] Thus, the important field gradient effects are already included in a dipole–dipole polarizability derivative calculation for the supermolecular system.

V Higher-order properties and their relevance to SERS

Most studies of surface-enhanced vibrational spectroscopy rely on linear Raman properties. However, recently surface-enhanced vibrational Raman optical activity and surface-enhanced hyper-Raman scattering have gained renewed interest. Both methods depend nonlinearly on the interactions between the molecule with the surface and it is expected that electronic structure methods will play an essential role in providing a detailed understanding.

A Surface-enhanced vibrational Raman optical activity

Vibrational Raman optical activity (VROA) measures the small differences in the Raman intensities of chiral molecules in right- and left-circularly polarized incident light.[122–124] Since VROA is sensitive to chirality it can provide information about the secondary and tertiary structure of proteins. Therefore, VROA has great potential for studying large bio-molecules in aqueous solution.[125–127] While VROA has proved to be a valuable tool in biomolecular research, the method is hampered by the low signal intensity (around a thousand times weaker than the already weak Raman intensities). Surface enhanced Raman optical activity (SEROA) scattering is proposed to give large VROA signals due to both a SERS-like enhancement of the overall scattering and enhancements from a large electric field gradient at the metal surface.[128–130] SEROA is a very new technique and only a few experimental studies have been reported.[131–133] So far, no experiments have reported enhancement factors for SEROA.

Theoretically, Janesko and Scuseria devised a method to determine SEROA by combining the electromagnetic response of orientationally-averaged model substrates with Raman optical activity expressions.[129] This model was based on the earlier electromagnetic theory of Efrima.[128] However, so far there have been no studies of the chemical effect on SEROA. Recently the TDDFT method used to study SERS has been extended to treat resonant VROA effects.[134] This enables a consistent treatment of both the electromagnetic and chemical mechanisms and is therefore a useful approach for getting a microscopic understanding of SEROA.

B Surface-enhanced hyper-Raman scattering and other nonlinear optical properties

Hyper-Raman scattering (HRS) is a nonlinear analog to Raman scattering in which the emitted photon is shifted by a vibrational quantum relative to the second harmonic of the incident radiation.[135] Due to different selection rules, HRS can probe vibrations that are forbidden in Raman scattering. However, HRS is extremely weak with intensities that are many orders of magnitude weaker than Raman cross sections for typical laser intensities. Similar to Raman scattering, HRS can be strongly enhanced for molecules adsorbed on metal surfaces, a process known as surface-enhanced hyper-Raman scattering (SEHRS).[102,136–139] The electromagnetic field enhancement in SEHRS is given by $|E(\omega)|^4|E(2\omega)|^2$. Since the field enhancement is dominated by the plasmon resonance at ω, one would expect the enhancement to be similar to what is found for SERS. However, the surface enhancement factors in SEHRS have been estimated to be of the order of 10^{12}–10^{14}, which is significantly larger than one would expect from the electromagnetic field enhancement.[102,137] This indicates a stronger contribution from the chemical enhancement, and it has been suggested that this might be due to more important excited-state charge transfer transitions for molecules on a surface than for the same molecules in solution.[102]

Electronic structure methods have in a few cases been applied to calculate the normal hyper-Raman scattering intensities[102,140,141] and compared with experimental SEHRS results. Although these calculations did not include metal atoms and therefore could not explain the enhancement mechanism, they proved valuable for vibrational assignment and elucidation of selection rules which are sensitive to the orientation of the molecule with respect to the surface. This is particularly useful since SEHRS is more sensitive than SERS to the orientation of the molecule. However, so far there have been no theoretical attempts to explain the apparently large chemical enhancement in SEHRS.

Other nonlinear effects are of increasing interest in the spectroscopy of silver and gold nanoparticles. Second harmonic generation[142–144] and hyper-Rayleigh spectra[145–147] have both been of interest recently, and although there are experimental measurements which show plasmon excitation effects, theory has not, so-far, been used to study these phenomena. Very recently, four wave mixing experiments[148] and theory[149,150] involving the use of polymer (Kerr nonlinear material) coated silver and gold nanostructures have started to appear, thus providing a nonlinear scattering effect which is sensitive to molecular adsorbates on silver/gold particles. TDDFT theory has not yet been used to describe surface enhanced nonlinear optical processes, but we anticipate that such applications to these materials will provide new insights in the use of nonlinear dielectrics in combination with plasmon enhanced local field enhancements in the development of optical devices.

VI. Concluding remarks

We have shown how time-dependent electronic structure methods, which treat the molecule and the metal at the same

level of theory and include the full frequency dependence of the electrodynamic response, can describe the different enhancement mechanisms of SERS and their relation to other optical properties in a uniform way, thereby providing microscopic insights into SERS. However, there are several important challenges which need to be addressed before a complete description of SERS is possible. The extension of these methods to allow calculations on large nanoparticles is obviously necessary to achieve a realistic model of SERS. This is unfortunately not easily done since periodic boundary conditions cannot be applied. The correct treatment of long-range CT excitations (position and linewidth) of molecules interacting with metal surfaces which the present day TDDFT method cannot describe correctly will also be important for a complete theory. Another area where electronic structure methods are necessary is to describe the coupling between molecular resonances and plasmon resonances as this is essential for understanding resonance Raman effects in SERS. Also, methods that can describe techniques like SEROA, SEHRS and surface-enhanced fluorescence are likely to be dominated by new developments in electronic structure methods. Future developments in electronic structure methods are therefore likely to play an important role in constructing a complete theory of SERS and related phenomena.

Acknowledgements

We thank the DTRA JSTO Program (FA9550-06-1-0558) and the NSEC program of the National Science Foundation (grant EEC-0647560) for support of this research.

References

1 U. Kreibig and M. Vollmer, *Optical Properties of Metal Clusters*, Springer, Berlin, 1995.
2 K. L. Kelly, E. A. Coronado, L. Zhao and G. C. Schatz, *J. Phys. Chem. B*, 2003, **107**, 668–677.
3 Y. Xia and N. J. Halas, *MRS Bull.*, 2005, **30**, 338–348.
4 C. Murphy, T. Sau, A. Gole, C. Orendorff, J. Gao, L. Gou, S. Hunyadi and T. Li, *J. Phys. Chem. B*, 2005, **109**, 13857–13870.
5 B. Gates, Q. Xu, M. Stewart, D. Ryan, C. Willson and G. Whitesides, *Chem. Rev.*, 2005, **105**(4), 1171–1196.
6 X.-Z. Zhang, A. V. Whitney, J. Zhao, E. N. Hicks and R. P. Van Duyne, *J. Nanosci. Nanotechnol.*, 2006, **6**, 1–15.
7 J. Henzie, J. Barton, C. Stender and T. Odom, *Acc. Chem. Res.*, 2006, **39**(4), 249–257.
8 P. D. Jadzinsky, G. Calero, C. J. Ackerson, D. A. Bushnell and R. D. Kornberg, *Science*, 2007, **318**, 430–433.
9 K. Kneipp, H. Kneipp, I. Itzkan, R. R. Dasari and M. S. Feld, *Chem. Rev.*, 1999, **99**, 2957–2975.
10 C. A. Mirkin, R. L. Letsinger, R. C. Mucic and J. J. Storhoff, *Nature*, 1996, **382**, 607–609.
11 A. J. Haes, W. P. Hall, L. Chang, W. L. Klein and R. P. Van Duyne, *Nano Lett.*, 2004, **4**, 1029–1034.
12 C. R. Yonzon, C. L. Haynes, X. Zhang, J. T. Walsh Jr. and R. P. Van Duyne, *Anal. Chem.*, 2004, **76**, 78–85.
13 D. A. Schultz, *Curr. Opin. Biotechnol.*, 2003, **14**(1), 13–22.
14 Y.-W. Cao, R. Jin and C. A. Mirkin, *Science*, 2002, **297**, 1536–1540.
15 S. G. Penn, L. He and M. J. Natan, *Curr. Opin. Chem. Biol.*, 2003, **7**, 609–615.
16 M. Moskovits, *Rev. Mod. Phys.*, 1985, **57**, 783–826.
17 A. Campion and P. Kambhampati, *Chem. Soc. Rev.*, 1998, **27**, 241–250.
18 S. Link and M. A. El-Sayed, *Annu. Rev. Phys. Chem.*, 2003, **54**, 331.
19 M. Fleischman, P. J. Hendra and A. J. McQuillan, *Chem. Phys. Lett.*, 1974, **26**, 163–166.
20 D. L. Jeanmaire and R. P. Van Duyne, *J. Electroanal. Chem.*, 1977, **84**, 1–20.
21 M. G. Albrecht and J. A. Crieghton, *J. Am. Chem. Soc.*, 1977, **99**, 5215–5217.
22 S. M. Nie and S. R. Emory, *Science*, 1997, **275**, 1102–1106.
23 K. Kneipp, Y. Wang, H. Kneipp, L. T. Perelman, I. Itzkan, R. R. Dasari and M. S. Feld, *Phys. Rev. Lett.*, 1997, **78**, 1667–1670.
24 H. Xu, E. J. Bjerneld, M. Käll and L. Börjesson, *Phys. Rev. Lett.*, 1999, **83**, 4357–4360.
25 A. M. Michaels, M. Nirmal and L. E. Brus, *J. Am. Chem. Soc.*, 1999, **121**, 9932–9939.
26 G. C. Schatz and R. P. Van Duyne, in *Handbook of Vibrational Spectroscopy*, ed. J. M. Chalmers and P. R. Griffiths, John Wiley and Sons, Ltd, 2002, vol. 1, pp. 759–774.
27 G. C. Schatz, M. A. Young and R. P. Van Duyne, in *Topics in Applied Physics*, ed. K. Kneipp, M. Moskovits and H. Kneipp, Springer-Verlag, Berlin, Heidelberg, 2006, vol. 103, pp. 19–46.
28 W.-H. Yang, G. C. Schatz and R. P. Van Duyne, *J. Chem. Phys.*, 1995, **103**, 869–875.
29 A. Taflove and S. C. Hagness, *Computational electrodynamics: The finite-difference time-domain method*, Artech House, Boston, 2005.
30 L. L. Zhao, L. Jensen and G. C. Schatz, *Nano Lett.*, 2006, **6**, 1229–1234.
31 B. Nikoobakht, J. Wang and M. A. El-Sayed, *Chem. Phys. Lett.*, 2002, **366**, 17–23.
32 E. Hao and G. C. Schatz, *J. Chem. Phys.*, 2004, **120**, 357.
33 D. P. Fromm, A. Sundaramurthy, J. Schuck, G. Kino and W. E. Moerner, *Nano Lett.*, 2004, **4**, 957–961.
34 A. Otto, in *Topics of Applied Physics 54, "Light Scattering in Solids"*, ed. M. Cardona and G. Güntherodt, Springer, Berlin/Heidelberg, 1984, vol. IV, pp. 289–418.
35 J. Gersten and A. Nitzan, *J. Chem. Phys.*, 1980, **73**, 3023–3037.
36 E. C. Le Ru and P. G. Etchegoin, *Chem. Phys. Lett.*, 2006, **423**, 63–66.
37 L. Silberstein, *Philos. Mag.*, 1917, **33**, 521.
38 L. Jensen, P.-O. Åstrand, A. Osted, J. Kongsted and K. V. Mikkelsen, *J. Chem. Phys.*, 2002, **116**, 4001.
39 A. Vivoni, R. L. Birke, R. Foucault and J. R. Lombardi, *J. Phys. Chem. B*, 2003, **107**, 5547–5557.
40 D.-Y. Wu, S. Duan, B. Ren and Z.-Q. Tian, *J. Raman Spectrosc.*, 2005, **36**, 533–540.
41 G. Cardini and M. Muniz-Miranda, *J. Phys. Chem. B*, 2002, **106**(27), 6875–6880.
42 D.-Y. Wu, B. Ren, Y.-X. Jiang, X. Xu and Z.-Q. Tian, *J. Phys. Chem. A*, 2002, **106**(39), 9042–9052.
43 G. Cardini, M. Muniz-Miranda, M. Pagliai and V. Schettino, *Theor. Chim. Acta*, 2007, **117**, 451–458.
44 P. Johansson, *Phys. Chem. Chem. Phys.*, 2005, **7**, 475–482.
45 D. Y. Wu, M. Hayashi, S. H. Lin and Z. Q. Tian, *Spectrochim. Acta, Part A*, 2004, **60**, 137–146.
46 F. J. Adrian, *J. Chem. Phys.*, 1982, **77**(11), 5302–5314.
47 J. R. Lombardi, R. L. Birke, T. Lu and J. Xu, *J. Chem. Phys.*, 1986, **84**, 4174–4180.
48 J. R. Lombardi and R. L. Birke, *J. Chem. Phys.*, 2007, **126**, 244709.
49 W. L. Peticolas, D. P. Strommen and V. Lakshminarayanan, *J. Chem. Phys.*, 1980, **73**(9), 4185–4191.
50 J. F. Arenas, M. S. Woolley, I. L. Tocon, J. C. Otero and J. I. Marcos, *J. Chem. Phys.*, 2000, **112**(17), 7669–7683.
51 J. F. Arenas, J. Soto, I. L. Tocón, D. J. Fernández, J. C. Otero and J. I. Marcos, *J. Chem. Phys.*, 2002, **116**(16), 7207–7216.
52 J. F. Arenas, I. L. Tocón, J. C. Otero and J. I. Marcos, *J. Phys. Chem.*, 1996, **100**, 9254–9261.
53 S. Centeno, I. Lopez-Tocon, J. Arenas, J. Soto and J. Otero, *J. Phys. Chem. B*, 2006, **110**, 14916–14922.
54 S. Corni and J. Tomasi, *J. Chem. Phys.*, 2002, **116**(3), 1156–1164.
55 S. Corni and J. Tomasi, *Chem. Phys. Lett.*, 2001, **342**, 135.
56 P. K. Pandey and G. C. Schatz, *Chem. Phys. Lett.*, 1982, **88**, 193–197.
57 P. K. Pandey and G. C. Schatz, *J. Chem. Phys.*, 1984, **80**, 2959–2972.

58 H. Nakai and H. Nakatsuji, *J. Chem. Phys.*, 1995, **103**, 2286–2294.
59 M. E. Casida, in *Recent Advances in Density-Functional Methods*, ed. D. P. Chong, World Scientific, Singapore, 1995, p. 155.
60 M. E. Casida, in *Recent Developments and Applications of Modern Density Functional Theory*, ed. J. M. Seminario, Elsevier, Amsterdam, 1996.
61 P. Norman, D. M. Bishop, H. J. A. Jensen and J. Oddershede, *J. Chem. Phys.*, 2001, **115**, 10323.
62 X. Blasé and P. Ordejón, *Phys. Rev. B*, 2004, **69**, 085111.
63 L. Jensen, J. Autschbach and G. C. Schatz, *J. Chem. Phys.*, 2005, **122**, 224115.
64 S.-Y. Lee, *J. Chem. Phys.*, 1982, **76**, 3064–3074.
65 S.-Y. Lee, *J. Chem. Phys.*, 1983, **78**, 723–734.
66 L. Jensen, L. L. Zhao, J. Autschbach and G. C. Schatz, *J. Chem. Phys.*, 2005, **123**, 174110(1)–174110(11).
67 D. A. Long, *The Raman Effect*, Wiley, Chichester, 2001.
68 J. M. Schulman, R. Detrano and J. I. Musher, *Phys. Rev. A*, 1972, **5**, 1125–1131.
69 J. M. Schulman and R. Detrano, *Phys. Rev. A*, 1974, **10**, 1192–1197.
70 W. S. Schulman and J. M. Lee, *J. Chem. Phys.*, 1981, **74**, 4930–4935.
71 H. A. Kramers and W. Heisenberg, *Z. Phys.*, 1925, **31**, 681.
72 P. A. M. Dirac, *Proc. R. Soc. London, Ser. A*, 1927, **114**, 710.
73 E. J. Heller, R. L. Sundberg and D. Tannor, *J. Phys. Chem.*, 1982, **86**, 1822–1833.
74 J. Sue, Y. J. Yan and S. Mukamel, *J. Chem. Phys.*, 1986, **85**, 462–474.
75 A. B. Meyers, *Annu. Rev. Phys. Chem.*, 1998, **49**, 267–295.
76 D. M. Wood and N. W. Ashcroft, *Phys. Rev. B*, 1982, **25**, 6255.
77 A. Liebsch, *Phys. Rev. B*, 1993, **48**, 11317.
78 W. A. de Heer, *Rev. Mod. Phys.*, 1993, **65**, 611.
79 W. P. Halperin, *Rev. Mod. Phys.*, 1986, **58**, 533.
80 M. Alvarez, J. Khoury, T. Schaaff, M. Shafigullin, I. Vezmar and R. Whetten, *J. Phys. Chem. B*, 1997, **101**, 3706–3712.
81 S. Logunov, T. Ahmadi, M. El-Sayed, J. Khoury and R. Whetten, *J. Phys. Chem. B*, 1997, **101**, 3713–3719.
82 T. Schaaff, M. Shafigullin, J. Khoury, I. Vezmar, R. Whetten, W. Cullen, P. First, C. Gutierrez-Wing, J. Ascensio and M. Jose-Yacaman, *J. Phys. Chem. B*, 1997, **101**, 7885–7891.
83 V. Bonačić-Koutecký, P. Fantucci and J. Koutecký, *Chem. Rev.*, 1991, **91**, 1035.
84 M. Brack, *Rev. Mod. Phys.*, 1993, **65**, 677.
85 T. L. Haslett, K. A. Bosnick and M. Moskovits, *J. Chem. Phys.*, 1998, **108**, 3453–3457.
86 T. L. Haslett, K. A. Bosnick, S. Fedrigo and M. Moskovits, *J. Chem. Phys.*, 1999, **111**, 6456–6461.
87 K. A. Bosnick, T. L. Haslett, S. Fedrigo and M. Moskovits, *J. Chem. Phys.*, 1999, **111**, 8867–8870.
88 L. Peyser-Capadona, J. Zheng, J. I. Gonzalez, T.-H. Lee, S. A. Patel and R. M. Dickson, *Phys. Rev. Lett.*, 2005, **94**, 058301(1)–058301(4).
89 R. C. Price and R. L. Whetten, *J. Phys. Chem. B*, 2006, **110**, 22166–22171.
90 V. Bonačić-Koutecký, J. Pittner, M. Boiron and P. Fantucci, *J. Chem. Phys.*, 1999, **110**, 3876–3886.
91 V. Bonačić-Koutecký, V. Veyret and R. Mitrić, *J. Chem. Phys.*, 2001, **115**, 10450–10460.
92 K. Yabana and G. F. Bertsch, *Phys. Rev. A*, 1999, **60**, 3809–3814.
93 J. C. Idrobo, S. Öğüt and J. Jellinek, *Phys. Rev. B*, 2005, **72**, 085445-1-11.
94 F. Conus, V. Rodrigues, S. Lecoultre, A. Rydlo and C. Felix, *J. Chem. Phys.*, 2006, **125**, 024511.
95 S. Fredigo, W. Harbich and J. Buttet, *Phys. Rev. B*, 1993, **47**, 10706–10715.
96 L. L. Zhao, L. Jensen and G. C. Schatz, *J. Am. Chem. Soc.*, 2006, **128**, 2911–2919.
97 L. Jensen, L. L. Zhao and G. C. Schatz, *J. Phys. Chem. C*, 2007, **111**(12), 4756–4764.
98 A. Dreuw, J. L. Weisman and M. Head-Gordon, *J. Chem. Phys.*, 2003, **119**, 2943–2946.
99 P. Avouris and J. E. Demuth, *J. Chem. Phys.*, 1981, **75**, 4783–4794.
100 A. Otto, K. H. Frank and B. Reihl, *Surf. Sci.*, 1985, **163**, 140.
101 Q. Zhong, C. Gahl and M. Wolf, *Surf. Sci.*, 2002, **496**, 21–32.
102 J. T. Golab, J. R. Sprague, K. T. Carron, G. C. Schatz and R. P. Van Duyne, *J. Chem. Phys.*, 1988, **88**, 7942–7951.
103 L. Jensen and G. C. Schatz, *J. Phys. Chem. A*, 2006, **110**, 5973–5977.
104 P. Pyykkö, *Angew. Chem., Int. Ed.*, 2004, **43**, 4412.
105 R. M. Olson and M. S. Gordon, *J. Chem. Phys.*, 2007, **126**, 214310.
106 X. Gu, S. Bulusu, X. Li, X. Zeng, J. Li, X. Gong and L.-S. Wang, *J. Phys. Chem. C*, 2007, **111**, 8228–8232.
107 K. J. Taylor, C. L. Pettiette-Hall, O. Cheshnovsky and R. E. Smalley, *J. Chem. Phys.*, 1992, **96**, 3319.
108 S. Bulusu, X. Li, L.-S. Wang and X. C. Zeng, *Proc. Natl. Acad. Sci. U. S. A.*, 2006, **103**, 8326.
109 S. Bulusu, X. Li, L.-S. Wang and X. C. Zeng, *J. Phys. Chem. C*, 2007, **111**, 4190.
110 H. Häkkinen, M. Moseler, O. Kostko, N. Morgner, M. A. Hoffmann and B. von Issendorff, *Phys. Rev. Lett.*, 2004, **93**, 093401.
111 B. Yoon, P. Kosinen, B. Huber, O. Kostko, B. von Issendorff, H. Häkkinen, M. Moseler and U. Landman, *ChemPhysChem*, 2007, **8**, 157.
112 J. Li, X. Li, H.-J. Zhai and L.-S. Wang, *Science*, 2003, **299**, 864–867.
113 C. Aikens and G. Schatz, *J. Phys. Chem. A*, 2006, **110**(49), 13317–13324.
114 B. A. Collings, K. Athanassenas, D. Lacombe, D. M. Rayner and P. A. Hackett, *J. Chem. Phys.*, 1994, **101**, 3506.
115 M. Moskovits and D. P. DiLella, *J. Chem. Phys.*, 1980, **73**, 6068.
116 J. K. Sass, H. Neff, M. Moskovits and S. Holloway, *J. Phys. Chem.*, 1981, **85**, 621.
117 M. Moskovits and D. P. DiLella, *J. Chem. Phys.*, 1982, **77**, 1655.
118 A. M. Polubotko, *J. Raman Spectrosc.*, 2005, **36**, 522.
119 S. S. Perry, S. R. Hatch and A. Campion, *J. Chem. Phys.*, 1996, **104**, 6856.
120 G. S. Kedziora and G. C. Schatz, *Spectrochim. Acta, Part A*, 1999, **55**, 625.
121 C. M. Aikens and G. C. Schatz, unpublished work.
122 L. D. Barron, *Molecular Light Scattering and Optical Activity*, Cambridge University Press, Cambridge, 2nd edn, 2004.
123 L. D. Barron, L. Hecht, I. H. McColl and E. W. Blanch, *Mol. Phys.*, 2004, **102**, 731–744.
124 W. Hug, in *Handbook of Vibrational Spectroscopy*, ed. J. M. Chalmers and P. R. Griffiths, John Wiley and Sons Ltd, Chichester, 2002, vol. 1, pp. 745–758.
125 F. Zhu, N. W. Isaacs, L. Hecht and L. D. Barron, *Structure*, 2005, **13**, 1409–1419.
126 F. Zhu, N. W. Isaacs, L. Hecht, G. E. Tranter and L. D. Barron, *Chirality*, 2006, **18**, 103–115.
127 L. D. Barron, *Curr. Opin. Struct. Biol.*, 2006, **16**, 638–643.
128 S. Efrima, *J. Chem. Phys.*, 1985, **83**(3), 1356–1362.
129 B. G. Janesko and G. E. Scuseria, *J. Chem. Phys.*, 2006, **125**(12), 124704.
130 P. Bour, *J. Chem. Phys.*, 2007, **126**(13), 136101.
131 S. Abdali, *J. Raman Spectrosc.*, 2006, **37**, 1341–1345.
132 H. Kneipp, J. Kneipp and K. Kneipp, *Anal. Chem.*, 2006, **78**, 1363–1366.
133 C. Johannessen, P. White and S. Abdali, *J. Phys. Chem.A*, 2007, **111**, 7771–7776.
134 L. Jensen, J. Autschbach, M. Krykunov and G. C. Schatz, *J. Chem. Phys.*, 2007, **127**, 134101.
135 L. D. Ziegler, *J. Raman Spectrosc.*, 1990, **21**, 769–779.
136 D. Murphy, K. U. von Raben, R. Chang and P. B. Dorain, *Chem. Phys. Lett.*, 1982, **85**, 43–47.
137 K. Kneipp, H. Kneipp and F. Seifert, *Chem. Phys. Lett.*, 1995, **233**, 519–524.
138 K. Kneipp, H. Kneipp, I. Itzkan, R. R. Dasari, M. S. Feld and M. Dresselhaus, *Top. Appl. Phys.*, 2002, **82**, 227–249.
139 W. Leng and A. M. Kelley, *J. Am. Chem. Soc.*, 2006, **128**, 3492–3493.
140 W.-H. Yang and G. C. Schatz, *J. Chem. Phys.*, 1992, **97**, 3831–3845.
141 W.-H. Yang, J. Hulteen, G. C. Schatz and R. P. Van Duyne, *J. Chem. Phys.*, 1996, **104**, 4313.

142 A. M. Moran, J. Sung, E. N. Hicks, R. P. Van Duyne and K. G. Spears, *J. Phys. Chem. B*, 2005, **109**, 4501–4506.
143 K. Tsuboi, S. Abe, S. Fukuba, M. Shimojo, M. Tanaka, K. Furuya, K. Fujita and K. Kajikawa, *J. Chem. Phys.*, 2006, **125**, 174703/1–174703/8.
144 C. Matranga and P. Guyot-Sionnest, *J. Chem. Phys.*, 2001, **115**, 9503–9512.
145 J. Nappa, I. Russier-Antoine, E. Benichou, C. Jonin and P.-F. Brevet, *Chem. Phys. Lett.*, 2005, **415**, 246–250.
146 I. Russier-Antoine, C. Jonin, J. Nappa, E. Benichou and P.-F. Brevet, *J. Chem. Phys.*, 2004, **120**, 10748–10752.
147 E. C. Hao, G. C. Schatz, R. C. Johnson and J. T. Hupp, *J. Chem. Phys.*, 2002, **117**, 5963–5966.
148 W. Dickson, G. A. Wurtz, P. Evans, D. O'Connor, R. Atkinson, R. Pollard and A. V. Zayats, *Phys. Rev. B*, 2007, **76**, 115411/1–115411/6.
149 N.-C. Panoiu and R. Osgood, *Nano Lett.*, 2004, **4**, 2427–2430.
150 X. Wang, G. C. Schatz and S. K. Gray, *Phys. Rev. B*, 2006, **74**, 195439/1–195439/5.